Eur. Phys. J. C (2026) 86:167
https://doi.org/10.1140/epjc/s10052-026-15385-w

THE EUROPEAN PHYSICAL JOURNAL C

Regular Article - Theoretical Physics

Dynamics of spinning particles around charged black holes in Bumblebee gravity

Jie Li[1,a], **Yi Zhu**[1], **Bo Yang**[2]

[1] School of Science, Hunan Institute of Technology, Hengyang 421002, China
[2] School of Mathematics and Physics, University of South China, Hengyang 421001, China

Received: 26 November 2025 / Accepted: 31 January 2026

Abstract In this paper, we investigate the motion and stability of spinning particles around a charged black hole in Bumblebee gravity. The trajectories of the particle are computed using the Mathisson–Papapetrou–Dixon equations, and the parameters of the innermost stable circular orbit (ISCO) are determined from the radial effective potential. The results show that the particle's spin and the black hole's parameters significantly influence the structure of the effective potential, thereby affecting the particle's orbital dynamics and stability. Orbital simulations show that when the particle is confined within a potential well, increasing its spin or the black hole's charge broadens the radial motion range, with the apocenter moving outward and the pericenter inward. At the same time, the Lorentz-violating (LV) parameter affects the radial motion range differently for particles with positive and negative spin. ISCO analysis further indicates that as the particle's spin and the black hole's charge increase, the radius, energy, and angular momentum of ISCO decrease. The effect of the LV parameter on the ISCO depends on the spin direction: increasing LV parameter for positively spinning particles brings the ISCO closer to the black hole, while negatively spinning particles exhibit the opposite trend.

1 Introduction

Einstein's general theory of relativity is currently the most successful theory describing gravity and has been rigorously verified through a series of experimental and observational tests, such as Mercury's perihelion precession, light deflection, gravitational redshift, and radar echo delay. Recent observations of gravitational waves from binary black hole mergers [1–3] and the shadows of supermassive black holes M87* [4–6] and SgrA* [7,8] provide further compelling support for general relativity. Despite its remarkable success in explaining numerous astrophysical phenomena, certain observational results suggest limitations within the theory. To better explain large-scale cosmic observations, scholars have proposed introducing new exotic matter dark matter and dark energy [9–11] within the framework of general relativity. However, to date, we have not directly detected dark matter or dark energy. Furthermore, one of the central aims of modern physics is to establish a unified framework for the four fundamental forces. Since general relativity cannot be consistently reconciled with quantum mechanics, numerous efforts have been devoted to modifying it, ultimately giving rise to the pursuit of quantum gravity.

In the study of quantum gravity, it is necessary to reexamine the fundamental symmetries in physics. Lorentz symmetry, as a cornerstone of both the standard model and general relativity, has long been regarded as strictly conserved. However, recent theoretical investigations indicate that this symmetry may be violated at the Planck scale (around 10^{19} GeV) [12] implying that it does not hold exactly at extremely high energy regimes. Furthermore, experimental observations suggest possible signatures of Lorentz symmetry breaking under high-energy conditions [13,14]. Consequently, various theoretical frameworks incorporating Lorentz-violating effects have been proposed, among which the Bumblebee gravity model is one of the simplest [15]. Within this theoretical framework, the vector field acquires a nonzero vacuum expectation value through its self-interaction potential, thereby inducing spontaneous breaking of Lorentz symmetry. Recently, a variety of black hole solutions have been obtained in Bumblebee gravity, including slowly rotating Kerr-like solutions [16], Schwarzschild-like solutions [17], de Sitter Schwarzschild solutions [18], Gauss–Bonnet terms solutions [19], and solutions with a global monopole [20]. In

[a] e-mail: lje@hnit.edu.cn (corresponding author)

Published online: 21 February 2026

addition, related wormhole solutions have also been explored in the literature [21].

In the past few years, various properties of black holes in Bumblebee gravity have been extensively studied. Ovgun et al. investigated the gravitational lensing effects of black holes in this framework and showed that the Bumblebee field parameters significantly affect the light deflection, providing a potential avenue to test Lorentz symmetry breaking through optical observations [21]. Jha et al. studied the motion of particles in this spacetime background and found that the Lorentz-violating factor affects the perihelion precession, while the orbital period for circular orbits remains unchanged [22]. Subsequently, other aspects of this spacetime have also been widely explored, including greybody factors [23,24], shadows [25,26], gravitational waves [27], thermodynamic properties [28–30] and quasinormal modes [31,32]. Recently, Liu et al. presented slowly rotating charged black hole solutions in Bumblebee gravity and investigated the structure of their shadows [33], and subsequent studies further analyzed the motion of particles [34,35], scalar quasinormal modes [36], greybody factors [37], strong lensing and Hawking spectra [38] in this spacetime.

The innermost stable circular orbit (ISCO) is one of the most significant topics in black hole physics, representing the smallest circular orbit where a particle can remain in stable motion around a black hole. The key ISCO parameters-radius ($r_{\rm ISCO}$), angular momentum ($l_{\rm ISCO}$), and energy ($e_{\rm ISCO}$)-play an essential role in studying the structure of accretion disks and the characteristics of gravitational wave emission. Early studies mainly focused on the ISCO behavior of nonspinning particles in various black hole spacetimes [39–49]. With deeper investigations, it was found that the coupling between a particle's spin and the gravitational field causes its motion to deviate from a geodesic path, thereby significantly influencing the ISCO location and related parameters.

The dynamics of spinning particles in Schwarzschild and Kerr geometries have been systematically analyzed [50]. Subsequently, approximate analytical expressions for ISCO parameters under small-spin corrections were derived [51]. Zhang et al. explored the properties of the ISCO in Kerr-Newman spacetime in the superluminal limit [52], incorporating the effects of particle charge. In recent years, extensive studies have further extended ISCO analyses for spinning particles in various modified or generalized gravitational backgrounds, making it an important area for probing the dynamics in strong-gravity regions [53–73]. In this paper, we analyze how spinning particles behave in circular orbits around the charged black hole in Bumblebee gravity.

The structure of this paper is as follows: In Sect. 2, we briefly review the charged black hole in Bumblebee gravity, and discuss its horizon structure in detail. Section 3 primarily presents the equations of motion for spinning particles in a general context, while Sect. 4 analyzes the dynamical properties of spinning test particles around a charged black hole in Bumblebee gravity, including the effective potential and the physical parameters of ISCO. Conclusions are given in Sect. 5. We use the natural units in which $G = c = 1$.

2 Charged black hole in Bumblebee gravity

In the bumblebee model, an additional vector field B_μ is introduced, which acquires a nonzero vacuum expectation value, thereby extending general relativity. The dynamics of this vector field lead to a spontaneous breaking of Lorentz symmetry. The action of the bumblebee gravity can be written as:

$$S = \int d^4x\sqrt{-g}\Big[\frac{1}{2\kappa}(R-2\Lambda) - \frac{1}{4}B_{\mu\nu}B^{\mu\nu} + \frac{\xi}{2\kappa}B^\mu B^\nu R_{\mu\nu} - V(B^\mu B_\nu \pm \bar{b}^2) + \mathcal{L}_M\Big], \tag{1}$$

where $\kappa = 8\pi$ is the gravitational coupling constant, $\mathcal{L}_M$ is the corresponding Lagrangian density, Λ represent the cosmological constant, $\mathcal{R}$ is the Ricci scalar, and ξ represents the non minimal coupling constant between the bumblebee field and gravity. The potential V and the bumblebee field strength $B_{\mu\nu}$ are defined by

$$B_{\mu\nu} \equiv \partial_\mu B_\nu - \partial_\nu B_\mu, \quad V \equiv V(B^\mu B_\nu \pm \bar{b}^2). \tag{2}$$

Here, b^2 is a positive real constant. The potential reaches its minimum at $B_\mu B^\mu = \mp b^2$, where the bumblebee field acquires a nonzero vacuum expectation value $B_\mu = b_\mu$. Within the framework of bumblebee gravity, to construct a charged black hole solution, the electromagnetic field is introduced as the matter source and is assumed to be non-minimally coupled to the bumblebee vector field. $\mathcal{L}_M$ can be expressed as:

$$\mathcal{L}_M = \frac{1}{2\kappa}(F^{\mu\nu}F_{\mu\nu} + \chi F^{\alpha\beta}F_{\alpha\beta}B_\mu B^\mu), \tag{3}$$

where χ is the coupling constant between the vector field and the electromagnetic field. The electromagnetic field tensor $F^{\mu\nu}$ is defined in terms of the gauge potential A_μ

$$F^{\mu\nu} \equiv \partial_\mu A_\nu - \partial_\nu A_\mu, \quad A_\mu = (\phi(r), 0, 0, 0). \tag{4}$$

The field equations result from performing a variation of Eq. (1) with respect to the metric

$$G_{\mu\nu} + \Lambda g_{\mu\nu} = \kappa T^B_{\mu\nu} + \kappa T^M_{\mu\nu}, \tag{5}$$

where

$$T^B_{\mu\nu} = \frac{\xi}{\kappa}\Big[\frac{1}{2}B^\alpha B^\beta R^{\alpha\beta}g_{\alpha\beta} + \frac{1}{2}\nabla_\alpha\nabla_\mu(B^\alpha B_\nu) + \frac{1}{2}\nabla_\alpha\nabla_\nu(B^\alpha B_\mu) - B_\mu B^\alpha R_{\alpha\nu} - B_\nu B^\alpha R_{\alpha\mu}$$

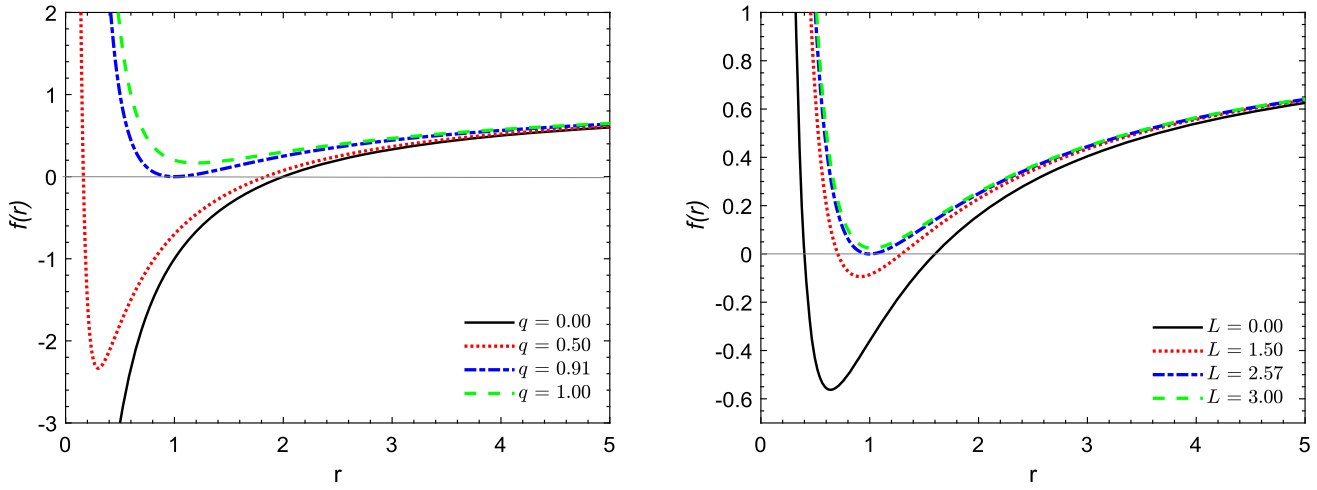

Fig. 1 The radial dependence of the lapse function $f(r)$ for various values of the LV parameter L and the charge q

$$
\begin{aligned}
&-\frac{1}{2}\nabla^2(B_\mu B_\nu)-\frac{1}{2}g_{\mu\nu}\nabla_\alpha\nabla_\beta(B^\alpha B^\beta)\Big]\\
&+2V'B_\mu B_\nu+B^\alpha_\mu B_{\nu\alpha}-\Big(V+\frac{1}{4}B_{\alpha\beta}B^{\alpha\beta}\Big)g^{\mu\nu},\\
T^M_{\mu\nu}=&\frac{1}{\kappa}\Big[(1+\chi\bar{b}^2)\Big(2F^{\mu\alpha}F^\alpha_\nu-\frac{1}{2}g_{\mu\nu}F^{\alpha\beta}\Big)F_{\alpha\beta}\Big)\\
&+\chi B_\mu B^\nu F^{\alpha\beta}\Big)F_{\alpha\beta}\Big].
\end{aligned}
\tag{6}
$$

By performing a variation of the action with respect to B_μ and A_μ, their corresponding field equations can be obtained, respectively:

$$
\nabla_\mu B^{\mu\nu}-2\Big(V'B^\nu-\frac{\xi}{2\kappa}B^\mu R^{\mu\nu}-\frac{\chi}{2\kappa}B^\nu F^{\alpha\beta}F_{\alpha\beta}\Big)=0,
\tag{7}
$$

and

$$
\nabla_\mu(F^{\mu\nu}+\chi B_\alpha B^\alpha F^{\mu\nu})=0.
\tag{8}
$$

Based on the above equations,charged black hole solution in the bumblebee gravity frame can be expressed as

$$
ds^2=-f(r)dt^2+\frac{1+L}{f(r)}dr^2+r^2(d\theta^2+sin^2\phi),
\tag{9}
$$

where

$$
f(r)=1-\frac{2M}{r}+\frac{2(1+L)q^2}{(2+L)r^2}.
\tag{10}
$$

where $L=\xi\bar{b}^2$ is Lorentz-violating (LV) parameter and q is the charge of the black hole. For the metric described above, if the LV parameter is zero, the spacetime reduces to the Reissner–Nordström black hole solution. When both the LV parameter and charge parameter vanish (i.e., $L=0$ and $q=0$), the structure degenerates into the standard Schwarzschild black hole.

The event horizon is determined by the condition $f(r)=0$. Figure 1 illustrates the behavior of $f(r)$ as a function of the radial coordinate r. In the left panel, we fix $L=0.5$ and compare cases with different charge parameters q. When $q=0$, $f(r)$ increases monotonically with r and crosses zero at one point, corresponding to the event horizon of the black hole. As q increases, the equation has two roots, corresponding to the Cauchy horizon and the event horizon, respectively. When $q=0.91$, the zero point coincides with the minimum of $f(r)$, indicating the extremal black hole case. For $q=1$, the equation has no real roots, implying the disappearance of the event horizon and the absence of a black hole solution. The right panel shows the behavior for a fixed $q=0.5$ with varying L. The results indicate that for the Reissner–Nordström black hole ($L=0$), two horizons exist. When $L>2.57$, no real roots exist, and the structure of black hole vanishes.

Furthermore, the analysis shows that for each given charge q, there exists a critical parameter $L_{\max}$, corresponding to the extremal black hole configuration. By numerically solving $f(r)=0$ and $\frac{df}{dr}=0$, we obtain the dependence of L on q, as shown in Fig. 2. In this work, we focus only on black hole solutions with an event horizon; Therefore, the parameter range is restricted to $L\leq L_{\max}$, corresponding to the shaded region in the figure.

3 Equations of motion for a spinning particle

The motion equations for spinning particles involve additional variables related to the particle's spin and Riemann curvature tensor, unlike non-spinning particles which follow geodesic equations. The motion of spinning particles is described by the Mathisson–Papapetrou–Dixon (MPD) equations, which take the following form [74–76]

$$
\frac{dx^\mu}{d\tau}=v^\mu,
\tag{11}
$$

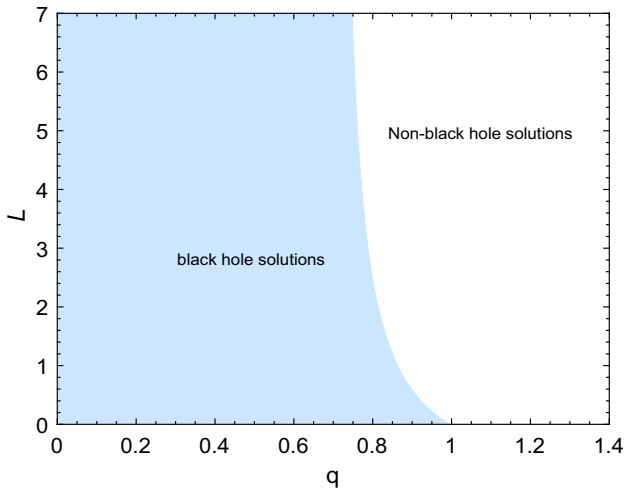

Fig. 2 The bounds on the LV parameter and the charge parameter are shown for charged black hole in Bumblebee gravity

$$\frac{Dp^{\mu}}{D\tau} = -\frac{1}{2}R^{\mu}_{\nu\alpha\beta}v^{\nu}S^{\alpha\beta}, \tag{12}$$

$$\frac{DS^{\mu\nu}}{D\tau} = P^{\mu}v^{\nu} - P^{\nu}v^{\mu}, \tag{13}$$

where $\frac{D}{D\lambda} \equiv u^{\mu}\nabla_{\mu}$ is the covariant derivative along the trajectory, and λ is the affine parameter. The spin tensor, which is antisymmetric ($S^{\mu\nu} = -S^{\nu\mu}$), describes the particle's spin. The Riemann curvature tensor is represented by $R^{\mu}_{\nu\rho\sigma}$, while the particle S momentum vector and four-velocity are given by P^{μ} and v^{μ}, respectively. The relationship between the spin vector S^{μ} and spin tensor $S^{\mu\nu}$ is given by:

$$S_{\mu} = \frac{1}{2}\epsilon_{\mu\nu\alpha\beta}u^{\nu}S^{\alpha\beta}, \tag{14}$$

$$S^{\mu\nu} = -\epsilon^{\mu\nu\alpha\beta}S_{\alpha}u_{\beta}, \tag{15}$$

where $\epsilon^{\mu\nu\alpha\beta}$ is Levi-Civita alternating symbol, and m is called the total resting mass.

Analyzing the degrees of freedom in the variables $S^{\mu\nu}$, P^{μ}, and u^{μ} appearing in Eqs. (12) and (13) shows that the system possesses 14 independent components, whereas the equations themselves provide only 10 independent constraints. Consequently, the system remains underdetermined. This indeterminacy arises from the relativistic fact that the center of mass of a spinning body depends on the observer s reference frame. To render the system well-defined, an additional constraint, known as the spin-supplementary condition, must be imposed. Several such conditions have been proposed in the literature. In this work, we adopt the Tulczyjew spin-supplementary condition, given by

$$P_{\mu}S^{\mu\nu} = 0. \tag{16}$$

Combining MPD equations and the Tulczyjew condition, one can determine the spin S and mass m of the particle

$$m^2 = -P^{\mu}P_{\mu}, \tag{17}$$

$$S^2 = \frac{1}{2}S^{\mu\nu}S_{\mu\nu}. \tag{18}$$

We consider an idealized case in which the spinning particle is confined to the equatorial plane of a black hole. Under these conditions, Eq. (15) shows that only specific components of the spin tensor remain nonzero, given by

$$\begin{aligned} S^{tr} &= -S^{rt} = -\frac{SP_{\phi}}{m}\frac{1}{\sqrt{-g_{tt}g_{rr}g_{\phi\phi}}}, \\ S^{t\phi} &= -S^{\phi t} = -\frac{SP_{r}}{m}\frac{1}{\sqrt{-g_{tt}g_{rr}g_{\phi\phi}}}, \\ S^{r\phi} &= -S^{\phi r} = -\frac{SP_{t}}{m}\frac{1}{\sqrt{-g_{tt}g_{rr}g_{\phi\phi}}}. \end{aligned} \tag{19}$$

where $g_{\mu\nu}$ is the metric tensor in the Bumblebee gravity. The conserved quantities for a spinning particle are modified by spin-curvature interaction, and their relation to a Killing vector $\mathcal{K}^{\mu}$ is expressed as

$$\mathcal{C} = \mathcal{K}^{\mu}P_{\mu} - \frac{1}{2}S^{\mu\nu}\mathcal{K}_{\mu;\nu}. \tag{20}$$

In the spherically symmetric black hole background described by the metric (9), the spacelike Killing vector $\xi^{\phi} = \frac{\partial}{\partial\phi}$ and the timelike Killing vector $\xi^{t} = \frac{\partial}{\partial t}$ correspond to total angular momentum and the conserved energy, respectively, and their expressions are as follows

$$\begin{aligned} E &= -P_t - \frac{1}{2}\frac{SP_{\phi}}{m}\frac{g_{tt,r}}{\sqrt{-g_{tt}g_{rr}g_{\phi\phi}}}, \\ J &= P_{\phi} - \frac{1}{2}\frac{SP_{t}}{m}\frac{g_{\phi\phi,r}}{\sqrt{-g_{tt}g_{rr}g_{\phi\phi}}}. \end{aligned} \tag{21}$$

Using the above expressions, we can further obtain the components of the four-momentum

$$P_t = \frac{-E - SAJ}{1 - S^2C}, \tag{22}$$

$$P_{\phi} = \frac{J - SBE}{1 - S^2C}, \tag{23}$$

where

$$\begin{aligned} A &= \frac{g_{tt,r}}{2\sqrt{-g_{tt}g_{rr}g_{\phi\phi}}}, \\ B &= \frac{g_{\phi\phi,r}}{2\sqrt{-g_{tt}g_{rr}g_{\phi\phi}}}, \\ C &= -AB = \frac{g_{tt,r}g_{\phi\phi,r}}{4g_{tt}g_{rr}g_{\phi\phi}}. \end{aligned} \tag{24}$$

Based on the constraint provided by Eq. (17), we can obtain

$$g^{tt}P_t^2 + g_{rr}(P^r)^2 + g^{\phi\phi}P_{\phi}^2 = -m^2. \tag{25}$$

Thus, the radial component of the momentum P^r can be determined

$$(P^r)^2 = -\frac{1}{g_{rr}}\Big[m^2 + g^{tt}P_t^2 + g^{\phi\phi}P_\phi^2\Big], \tag{26}$$

In our analysis, we introduce the dimensionless quantities e, j, and s, which are defined as $e = \frac{E}{m}$, $j = \frac{J}{m}$, $s = \frac{S}{m}$. With Eqs. (22) and (23) substituted into Eq. (26), the radial momentum P^r can be reformulated as

$$(P^r)^2 = \frac{\beta}{\alpha}(e - V_{eff}^+)(e - V_{eff}^-), \tag{27}$$

$$V_{eff}^{\pm} = -\frac{\delta j}{2\beta} \pm \sqrt{\Big(\frac{\delta j}{2\beta}\Big)^2 + \Big(\frac{\rho}{\beta} - \frac{\sigma j^2}{\beta}\Big)}, \tag{28}$$

where

$$\begin{aligned}
\alpha &= g_{rr}\Big(1 - \frac{s^2 g_{tt,r} g_{\phi\phi,r}}{4 g_{tt} g_{rr} g_{\phi\phi}}\Big)^2,\\
\beta &= -g^{tt} + \frac{s^2 g^{\phi\phi}(g_{\phi\phi,r})^2}{4 g_{tt} g_{rr} g_{\phi\phi}},\\
\delta &= \frac{s(g^{tt} g_{tt,r} - g^{\phi\phi} g_{\phi\phi,r})}{\sqrt{-g_{tt} g_{rr} g_{\phi\phi}}},\\
\sigma &= -g^{\phi\phi} + \frac{s^2 g^{tt}(g_{tt,r})^2}{4 g_{tt} g_{rr} g_{\phi\phi}},\\
\rho &= m^2\Big(1 - \frac{s^2 g_{tt,r} g_{\phi\phi,r}}{4 g_{tt} g_{rr} g_{\phi\phi}}\Big)^2.
\end{aligned} \tag{29}$$

Notably, V_{eff}^+ indicates that the four-momentum points toward the future direction, whereas V_{eff}^- indicates that it points toward the past direction. Therefore, we only consider V_{eff}^+ as the effective potential.

From Eq. (13), we have

$$\frac{DS^{tr}}{D\lambda} = p^t u^r - p^r u^t, \tag{30}$$

$$\frac{DS^{t\phi}}{D\lambda} = p^t u^\phi - p^\phi u^t. \tag{31}$$

The choice of affine parameter does not affect the particle's trajectory, so we set it equal to the coordinate time t for simplicity. Under this assumption, the time component of the four-velocity becomes $u^t = 1$, and the radial and angular components are $u^r = \dot{r}$ and $u^\phi = \dot{\phi}$, respectively. With these substitutions, Eqs. (12) and (13) can be inserted into Eqs. (30) and (31) to yield the following expressions

$$p^t u^r - p^r = \frac{Ms}{2\sqrt{-g_{tt} g_{rr} g_{\phi\phi}}} g_{\phi v} R^v_{\alpha\beta\eta} u^\alpha S^{\beta\eta}, \tag{32}$$

$$p^t u^\phi - p^\phi = -\frac{Ms}{2\sqrt{-g_{tt} g_{rr} g_{\phi\phi}}} g_{rv} R^v_{\alpha\beta\eta} u^\alpha S^{\beta\eta}. \tag{33}$$

As a result, the radial and tangential velocities are represented by the following equation

$$\dot{r} = \frac{2\sqrt{-g_{tt} g_{rr} g_{\phi\phi}}\, p^r + \frac{Ms}{2\gamma} R_{\phi t\alpha\beta} S^{\beta\eta}}{p^t - \frac{Ms}{2\gamma} R_{\phi r\alpha\beta} S^{\beta\eta}}, \tag{34}$$

$$\dot{\phi} = \frac{p^\phi + \frac{Ms}{2\gamma} R_{rt\alpha\beta} S^{\beta\eta}}{p^t + \frac{Ms}{2\gamma} R_{r\phi\alpha\beta} S^{\beta\eta}}, \tag{35}$$

4 Dynamics of spinning particles around a charged black hole in Bumblebee gravity

4.1 The effective potential

Using notations given in Eq. (24), we obtain:

$$A = \frac{2(1+L^2)q^2 - (2+L)Mr}{r^4(2+L)\sqrt{1+L}}, \tag{36}$$

$$B = \frac{1}{\sqrt{1+L}},$$

$$C = \frac{Mr}{r^4(1+L)} - \frac{2q^2}{r^4(2+L)}. \tag{37}$$

Putting them into Eqs. (22) and (23), we can get time and angular components of P of spinning particle

$$P_t = \frac{J\sqrt{1+L}\big[(2+L)Mr - 2(1+L)q^2\big] - E(2+3L+L^2)r^4}{(2+3L+L^2)r^4 + \big[2(1+L)q^2 - (2+L)Mr\big]s^2},$$

$$P_\phi = \frac{J - Es/\sqrt{1+L}}{1 - \big(M/[r^3(1+L)] - 2q^2/[r^4(2+L)]\big)}$$

Finally, using Eq. (27) we find radial component of the four momentum

$$\begin{aligned}
\alpha &= \frac{\big[(2+3L+L^2)r^4 + 2(1+L)q^2s^2 - (2+L)Mrs^2\big]^2}{r^6\big[2+3L+L^2\big]\big[2(1+L)q^2 - (2+L)(2M-r)r\big]},\\
\beta &= \frac{(2+3L+L^2)r^4 - 2(1+L)q^2s^2 + 2(2+L)Mrs^2 - (2+L)r^2s^2}{r^2\big[1+L\big]\big[2(1+L)q^2 - (2+L)(2M-r)r\big]},\\
\delta &= \frac{8(1+L)q^2s - 2(2+L)(3M-r)rs}{r^2\sqrt{1+L}\big[2(1+L)q^2 - (2+L)(2M-r)r\big]},\\
\sigma &= -\frac{1}{r^2} + \frac{4\big[(2+L)Mr - 2(1+L)q^2\big]^2s^2}{r^6\big[2+3L+L^2\big]\big[2(1+L)q^2 - (2+L)(2M-r)r\big]},\\
\rho &= \frac{m^2\big[2(2+3L+L^2)r^4 + 2(1+L)q^2s^2 - (2+L)Mrs^2\big]^2}{r^8(1+L)^2(2+L)^2}.
\end{aligned} \tag{38}$$

By substituting the above expressions into Eq. (28), we obtain the effective potential of a spinning particle in Bumblebee gravity. It can be seen that the formula simultaneously involves the spin parameter s, the charge q, and the Lorentz-violating parameter L, all of which modify the specific values of the effective potential. In the spinless limit $s \to 0$, the effective potential reduces to that of a non-spinning test particle in the corresponding charged Bumblebee black hole spacetime. When $L \to 0$ and $q \to 0$, all expressions consistently recover the results of standard general relativity.

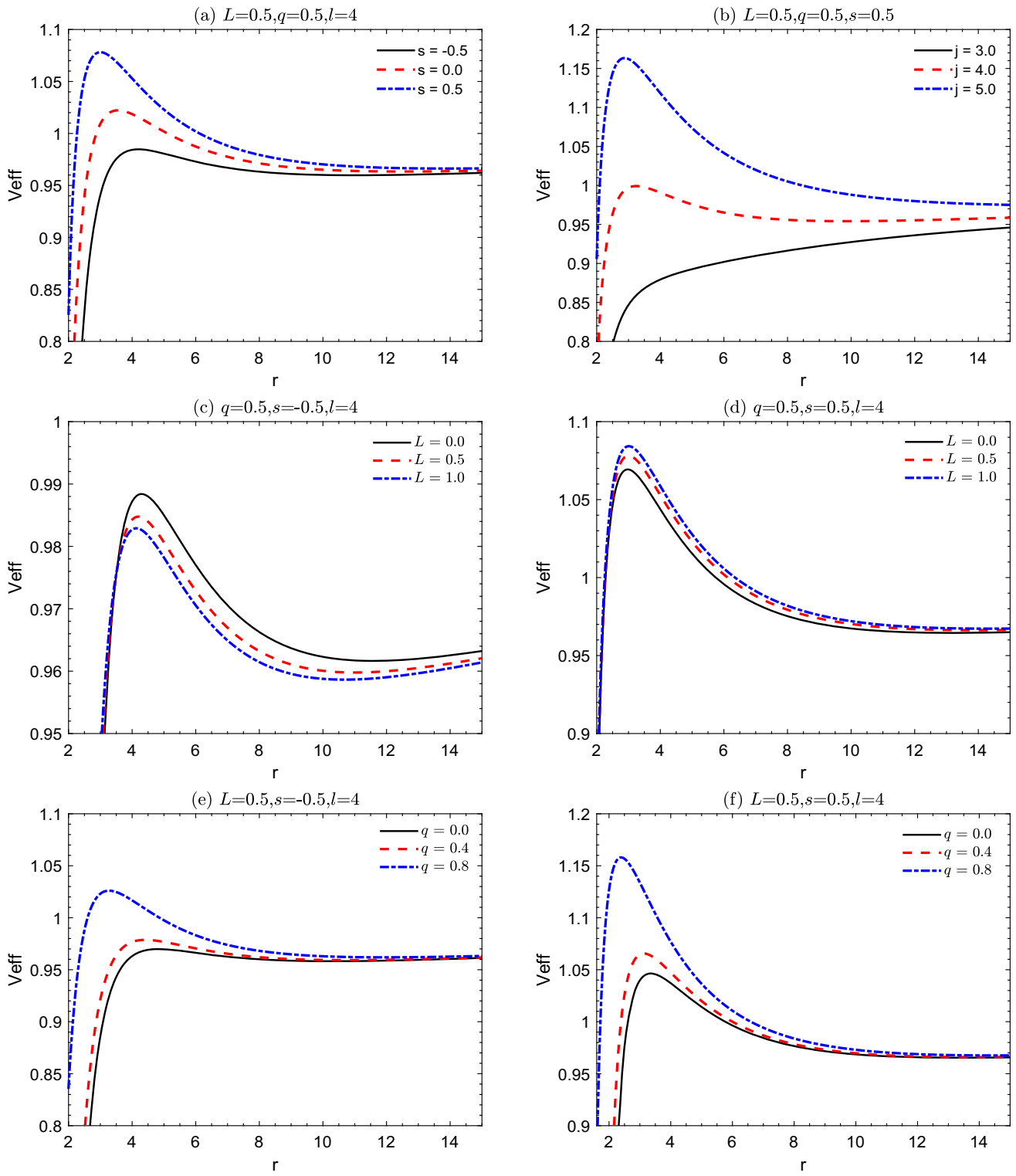

Fig. 3 Effective potential of spinning particles for different parameters around charged black hole in Bumblebee gravity

Figure 3 illustrates the effective potential profiles for different parameter values, where conserved angular momentum is expressed as $j = l + s$, with l representing orbital angular momentum. Overall, the effective potential curves exhibit two typical forms: one is a smooth, monotonic curve without extrema, indicating the absence of stable circular orbits; the other features both local maxima and minima, corresponding to the simultaneous existence of unstable and stable circular orbits. Figure 3a illustrates the effect of particle's spin on the effective potential, with fixed parameters $L = 0.5$, $q = 0.5$, and $l = 4$. Results indicate that

compared with spinless particles, the effective potential of spinning particles exhibits an overall upward trend with increasing spin parameter s, showing significant variation. Additionally, an increase in total angular momentum also elevates the peak of the effective potential, as shown in Fig. 3b. Figure 3c, d respectively illustrate the effect of the LV parameter L on the effective potential when the particle's spin is positive and negative. We observe that for positive s, increasing L from 0 to 1 significantly elevates the peak of the curve. Smaller L values correspond to lower effective potentials, while larger L values raise the entire curve, thereby altering the particle's motion characteristics. Conversely, for negative s, The influence of L on the effective potential exhibits the opposite behavior. Figure 3e, f illustrates the effect of the charge parameter q on the effective potential energy. Results indicate that as q increases, the peak of the curve rises and its shape changes significantly, indicating that the black hole's charge strongly affects the particle s orbital stability.

To intuitively illustrate the influence of different parameters on the motion of spinning particles, Fig. 4 presents the particle trajectories near the black hole under various parameter choices. The results show that when the particle is confined within the potential well, increasing its spin parameter or electric charge significantly modifies its radial motion interval. Specifically, the apocenter shifts outward and the pericenter moves inward, leading to a wider radial range. In addition, the effect of the LV parameter exhibits two distinct behaviors: when the particle spin is positive, increasing L enlarges the radial motion range, whereas for negative spin, increasing L reduces this range.

4.2 ISCO of the spinning particle

In this section, we investigate ISCO of charged black holes in Bumblebee gravity and analyze the effect of (s, q, L) on orbital parameters. According to the curve of V_{eff}, the following two equations are given

$$\frac{dV_{eff}}{d\tau} = 0, \qquad \frac{d^2V_{eff}}{dr^2} = 0. \tag{39}$$

We can use the above conditions to determine the ISCO of particles for the given values of the parameters s, q and L. However, there is an additional factor to be considered. In relativistic dynamics, the four-velocity u^μ determines the causal nature of a particle's worldline. For any massive particle, physically admissible motion must be timelike, satisfying $u^\mu u_\mu < 0$. The condition $u^\mu u_\mu = 0$ corresponds to the critical boundary between timelike and spacelike trajectories, while $u^\mu u_\mu > 0$ implies a spacelike motion, which would violate the causal structure of relativity and is therefore physically forbidden. For a non-spinning test particle, its motion is governed by the geodesic equation, and the four-velocity always satisfies the normalization condition $u^\mu u_\mu = -1$, which is strictly conserved along the trajectory. Thus, in the absence of spin, the particle's worldline remains timelike and cannot transition from a timelike to a spacelike trajectory. In contrast, within the MPD framework for spinning particles, the presence of spin-curvature coupling causes the four-velocity u^μ to no longer be strictly parallel to the four-momentum, and $u^\mu u_\mu$ is generally not conserved. For certain parameter values, the evolution of the trajectory may lead to $u^\mu u_\mu > 0$, at which point the particle s worldline becomes spacelike, corresponding to superluminal motion. To avoid such unphysical behavior, the boundary condition $u_\mu u^\mu = 0$ is introduced as a threshold, based on which the allowed range of spin values can be restricted.

$$\frac{u^2}{(u^t)^2} = g_{tt} + g_{rr}\dot{r}^2 + g_{\phi\phi}\dot{\phi}^2 < 0. \tag{40}$$

The critical value of s beyond which the particle s motion becomes superluminal can be obtained by numerically solving Eq. (39) and (40). Figure 5 illustrates how the maximum allowable spin $s_{\max}$ of a spinning particle varies with the black hole's charges q and the LV parameter L. It can be seen that, for a fixed q, the LV parameter and the maximum spin $s_{\max}$ exhibit an approximately linear increasing relationship. For a fixed L, $s_{\max}$ initially shows a monotonic decrease as q increases. However, when $q = 0.75$, $s_{\max}$ instead displays a monotonic increase with increasing q.

Next, we analyze the ISCO parameters of spinning particles around charged black hole in Bumblebee gravity. The upper panel of Fig. 6 shows how the ISCO of a spinning particle varies with its spin s in an uncharged black hole spacetime for different values of L. In the left panel, we set $L = 0$, corresponding to the Schwarzschild black hole. The vertical line at $s \approx 1.6518$ divides the curve into two regions: in the unshaded area, the velocity vector is timelike, and the motion is physically allowed, whereas in the shaded area, the velocity vector is spacelike, making the motion nonphysical. It can be seen that when $s = -2$, the ISCO radius is 8.2, and as the particle s spin increases, the ISCO radius gradually decreases; when the spin reaches its maximum value, the radius reduces to 2.6. At the same time, both the particle s energy and angular momentum decrease with increasing s.

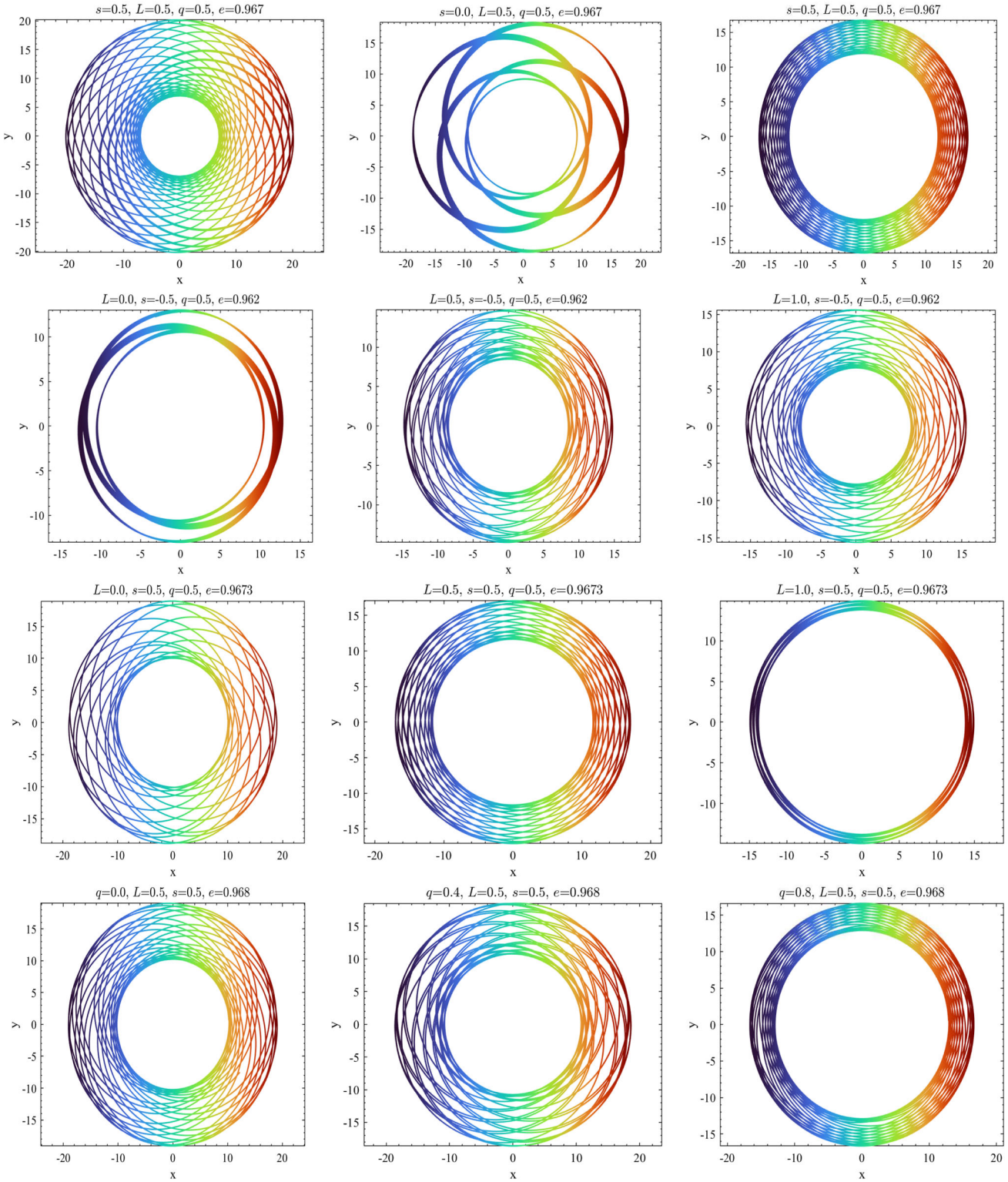

Fig. 4 Bounded trajectories of spinning particles for different parameters around charged black hole in Bumblebee gravity

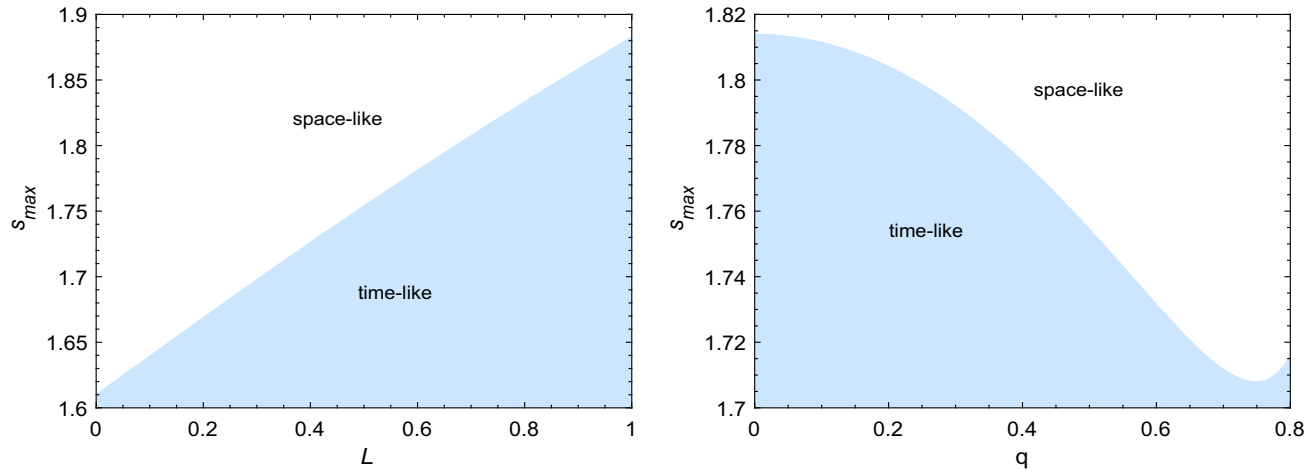

Fig. 5 Behavior of the maximum spin s_{max} for various values of the LV parameter L and the charge q

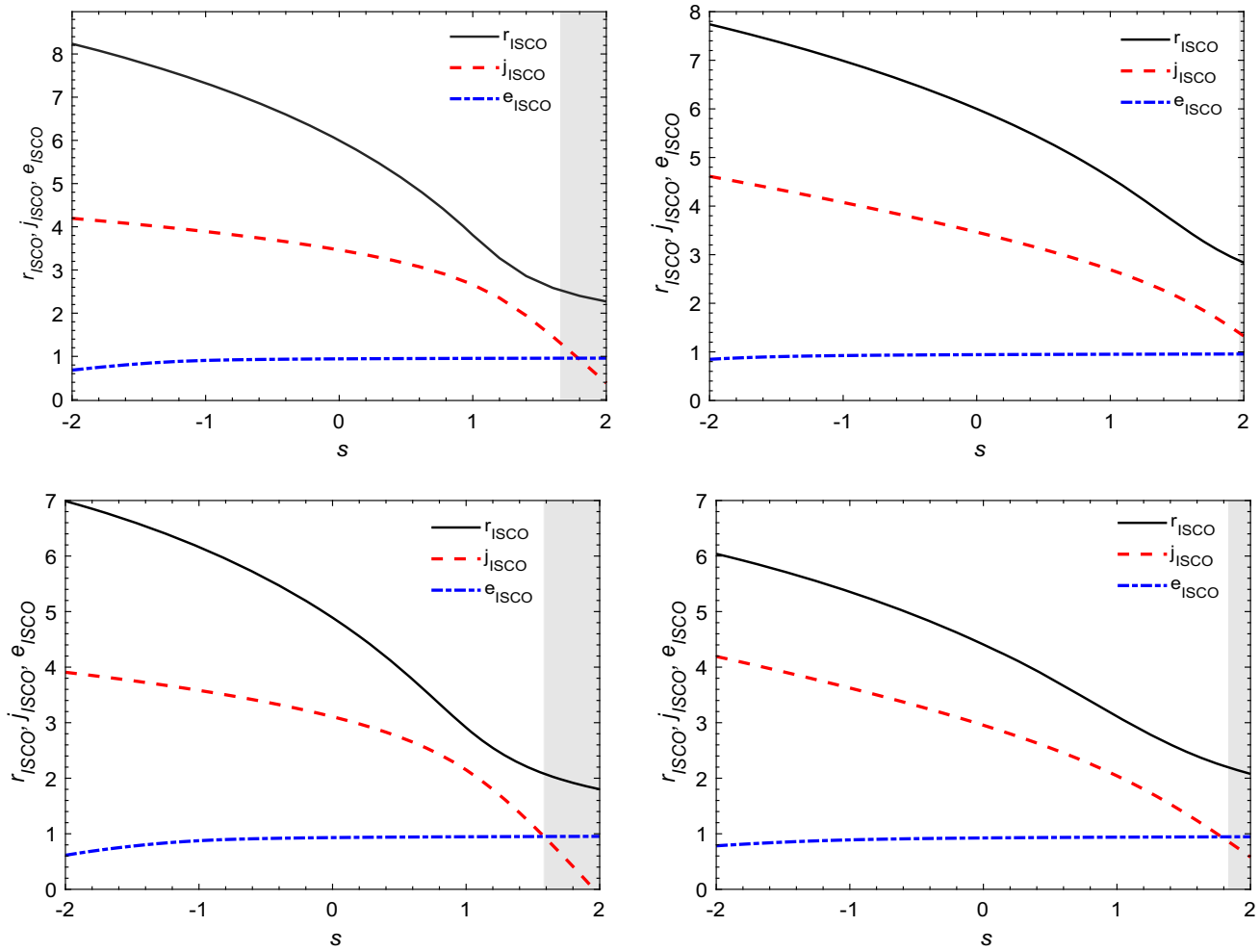

Fig. 6 Behavior of ISCO parameters as a function of spin for the spinning test particle around charged black holes in Bumblebee gravity

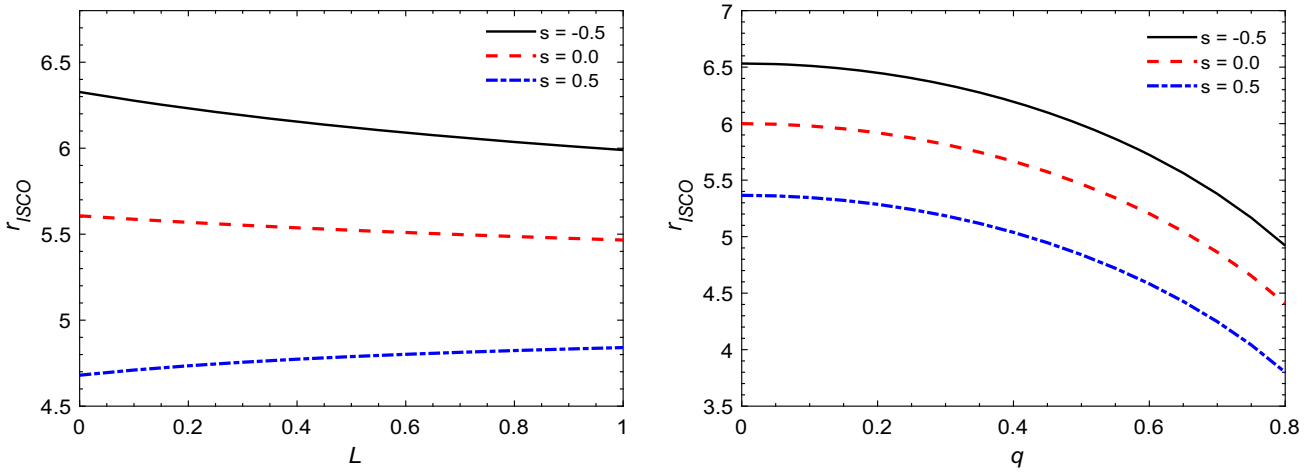

Fig. 7 Radius of the ISCO for spinning particles moving around charged black holes in Bumblebee gravity as function of the LV parameters L and q

We analyzed the effect of the LV parameter L on the ISCO parameters, as shown in the right panel, where $L = 1.0$ is adopted. For a particle with spin $s = -2$, the ISCO radius is approximately 7.8, which is smaller than that in the Schwarzschild black hole case; whereas for a particle with spin $s = 2$, the ISCO radius is about 2.8, larger than in the Schwarzschild case. To more clearly illustrate the influence of L, Fig. 7 shows the variation of the ISCO radius with respect to L. It can be observed that, when $s > 0$, the ISCO radius decreases monotonically as L increases, indicating that a larger L leads to a smaller stable circular orbit radius, allowing the particle to move closer to the black hole; conversely, when $s < 0$, the behavior is reversed.

The lower panel of Fig. 6 displays the orbital characteristics of spinning particles in the spacetime of a charged black hole. In the left panel, we set $L = 0$ and $q = 0.5$, corresponding to a Reissner–Nordström black hole. Compared to the Schwarzschild case, the particle's ISCO radius, angular momentum, and energy are all reduced; For $s = -2$, the orbital radius is approximately $r_{\rm ISCO} = 8.0$. Figure 7 illustrates the variation of the ISCO radius with charge q. The results indicate that the radius of stable circular orbits exhibits a continuous decreasing as charge increases. In the right panel, we set $L = 1$ and $q = 0.5$, corresponding to a Reissner–Nordström-like black hole in Bumble gravity. The results show that the effect of L on the ISCO is consistent with the trend observed in the Schwarzschild-like black hole.

5 Conclusions

In this paper, we systematically investigate the orbital dynamics and stability of spinning test particles around a charged black hole in Bumblebee gravity by analyzing the effective potential and the corresponding properties of the ISCO, and further examine how the particle's spin and the black hole's parameters influence the motion of spinning particles.

Analysis of the effective potential reveals that particle's spin plays a crucial role in determining the shape of the potential curve. As spin increases, the overall effective potential rises, making the potential barrier more pronounced. Similarly, an increase in total angular momentum also elevates the potential peak. The LV parameter L and charge q of the black hole significantly influence the potential structure. Increasing either parameter alters the shape of the potential curve, thereby affecting particle orbital behavior and stability. Orbital simulations reveal that confining particles within a potential well broadens the radial motion range when spin or charge increases shifting apocenters outward and pericenters inward. The LV parameter exhibits two distinct trends: increasing L expands the radial motion range for particles with positive spin, while increasing L contracts this range for particles with negative spin. The maximum permissible spin of the particle $s_{\rm max}$ is highly sensitive to both L and q. $s_{\rm max}$ increases approximately linearly with increasing L. However, with increasing charge, $s_{\rm max}$ initially decreases monotonically but then increases again with further charge increase beyond a specific charge value.

Regarding the ISCO, the analysis indicates that for an uncharged black hole, the ISCO radius, energy, and angular momentum all decrease as the particle's spin increases. When the spin reaches its maximum, the ISCO radius is significantly reduced, and both the particle's energy and angular momentum decrease accordingly. The introduction of the LV parameter affects the ISCO radius: for positive spin, increasing L reduces the ISCO radius, allowing the particle to orbit closer to the black hole, while for negative spin, the effect is reversed. In the case of a charged black hole, the particle's

ISCO radius, angular momentum, and energy are smaller than in the uncharged case and continue to decrease as the charge increases.

In summary, spinning particles and charge black holes are likely present in astrophysical systems, and Bumblebee gravity is an important Lorentz symmetry-breaking modification theory. We jointly considered the impact of charge and LV effects on the motion of spinning particles, showing how these effects collectively alter particle orbits in strong gravitational fields. These effects may be distinguishable in astronomical observations, especially in strong-field tests and high-precision gravitational wave detection. With the development of advanced gravitational wave detectors such as LIGO, Virgo, and LISA, we will be able to precisely measure ISCO information, including black hole's charge and LV effects, through gravitational wave signals. This will provide important support for understanding black hole systems and future research.

Acknowledgements This work was supported by the National Natural Science Foundation of China (Grant Nos. 12475057 and 12303079).

Data Availability Statement This manuscript has no associated data. [Authors' comment: Data sharing not applicable to this article as no datasets were generated or analysed during the current study.]

Code Availability Statement This manuscript has no associated code/software. [Authors' comment: Code/Software sharing not applicable to this article as no code/software was generated or analysed during the current study.]

Funded by SCOAP[3].

References

1. B.P. Abbott, R. Abbott, T.D. Abbott et al., Phys. Rev. Lett. **116**, 061102 (2016)
2. B.P. Abbott, R. Abbott, T.D. Abbott et al., Phys. Rev. Lett. **118**, 221101 (2017)
3. B.P. Abbott, R. Abbott, T.D. Abbott et al., Phys. Rev. Lett. **119**, 141101 (2017)
4. K. Akiyama, A. Alberdi, W.W. Alef et al., Astrophys. J. Lett. **875**, L1 (2019)
5. K. Akiyama, A. Alberdi, W.W. Alef et al., Astrophys. J. Lett. **875**, L4 (2019)
6. K. Akiyama, A. Alberdi, W.W. Alef et al., Astrophys. J. Lett. **875**, L6 (2019)
7. K. Akiyama, A. Alberdi, W.W. Alef et al., Astrophys. J. Lett. **930**, L12 (2022)
8. K. Akiyama, A. Alberdi, W.W. Alef et al., Astrophys. J. Lett. **930**, L17 (2022)
9. R.R. Caldwell, R. Dave, P.J. Steinhardt, Phys. Rev. Lett. **80**, 1582 (1998)
10. R.R. Caldwell, M. Kamionkowski, N.N. Weinberg, Phys. Rev. Lett. **91**, 071301 (2003)
11. Y.F. Cai, E.N. Saridakis, M.R. Setare et al., Phys. Rep. **493**, 1 (2010)
12. G. Amelino-Camelia, Living Rev. Relativ. **16**, 5 (2013)
13. A.S. Friedman, D. Leon, K.D. Crowley et al., Phys. Rev. D **99**, 035045 (2019)
14. C.G. Shao, Y.F. Chen, Y.J. Tan et al., Phys. Rev. Lett. **122**, 011102 (2019)
15. V.A. Kostelecky, S. Samuel, Phys. Rev. D **40**, 1886 (1989)
16. C. Ding, C. Liu, R. Casana, A. Cavalcante, Eur. Phys. J. C **80**, 178 (2020)
17. R. Casana, A. Cavalcante, F.P. Poulis, E.B. Santos, Phys. Rev. D **97**, 104001 (2018)
18. R.V. Maluf, J.C.S. Neves, Phys. Rev. D **103**, 044002 (2021)
19. C. Ding, X. Chen, X. Fu, Nucl. Phys. B **975**, 115688 (2022)
20. I. Güllü, V.P.Y.A. övgün, Ann. Phys
21. A. Övgün, K. Jusufi, I. Sakallı, Phys. Rev. D **99**, 024042 (2019)
22. S.K. Jha, H. Barman, A. Rahaman, J. Cosmol. Astropart. Phys. **2021**, 036 (2021)
23. K. Jusufi, I. Sakallı, Eur. Phys. J. C **81**, 501 (2021)
24. A. Uniyal, K. Jusufi, I. Sakallı, Eur. Phys. J. C **83**, 668 (2023)
25. S.K. Jha, A. Rahaman, Eur. Phys. J. C **81**, 345 (2021)
26. H.M. Wang, S.W. Wei, Eur. Phys. J. Plus **137**, 571 (2022)
27. K.M. Amarilo, M.B.F. Filho, A.A.A. Filho et al., Phys. Lett. B **855**, 138785 (2024)
28. R. Karmakar, D.J. Gogoi, U.D. Goswami, Phys. Dark Univ. **41**, 101249 (2023)
29. Z.F. Mai, R. Xu, D. Liang, L. Shao, Phys. Rev. D **108**, 024004 (2023)
30. Y.S. An, Phys. Dark Univ. **45**, 101520 (2024)
31. D.J. Gogoi, U.D. Goswami, J. Cosmol. Astropart. Phys. **2022**, 029 (2022)
32. X. Zhang, M. Wang, J. Jing, Sci. China Phys. Mech. Astron. **66**, 100411 (2023)
33. J.Z. Liu, W.D. Guo, S.W. Wei, Y.X. Liu, Eur. Phys. J. C **85**, 145 (2025)
34. M. Xu, J.B. Lu, R.N. Li et al., Class. Quantum Gravity **42**, 135008 (2025)
35. G. Mustafa, S.K. Maurya, P. Channuie et al., Phys. Dark Universe **47**, 101753 (2025)
36. J. de Oliveira, A.B. Pavan, K. Lin et al., Class. Quantum Gravity **42**, 235018 (2025)
37. Y.P. Singh, J. Choudhury, T.I. Singh et al., Eur. Phys. J. Plus **140**, 1118 (2025)
38. Y.P. Singh, N. Media, T.I. Singh, Eur. Phys. J. C **85**, 1223 (2025)
39. E. Hackmann, C. Lämmerzahl, V. Kagramanova et al., Phys. Rev. D **81**, 044020 (2010)
40. D. Pugliese, H. Quevedo, R. Ruffini, Phys. Rev. D **84**, 044030 (2011)
41. D. Pugliese, H. Quevedo, R. Ruffini, Phys. Rev. D **83**, 024021 (2011)
42. D. Pugliese, H. Quevedo, R. Ruffini, Phys. Rev. D **83**, 104052 (2011)
43. C. Chakraborty, Eur. Phys. J. C **74**, 2759 (2014)
44. S. Hod, Eur. Phys. J. C **74**, 2840 (2014)
45. O.B. Zaslavskii, Eur. Phys. J. C **75**, 403 (2015)
46. H.C. Lee, Y.J. Han, Eur. Phys. J. C **77**, 655 (2017)

47. G. Chartas, H. Krawczynski, L. Zalesky et al., Astrophys. J. **837**, 26 (2017)
48. M. Sharif, M. Shahzadi, Eur. Phys. J. C **77**, 363 (2017)
49. M.Y. Guo, P.C. Li, Eur. Phys. J. C **80**, 1 (2020)
50. S. Suzuki, K.I. Maeda, Phys. Rev. D **58**, 023005 (1997)
51. P.I. Jefremov, O.Y. Tsupko, G.S. Bisnovatyi-Kogan, Phys. Rev. D **91**, 124030 (2015)
52. Y.P. Zhang, B.M. Gu, S.W. Wei et al., Phys. Rev. D **94**, 124017 (2016)
53. Y.P. Zhang, S.W. Wei, P. Amaro-Seoane, J. Yang, Y.X. Liu, Eur. Phys. J. C **79**, 856 (2019)
54. M. Zhang, J. Jiang, Phys. Rev. D **101**, 104012 (2020)
55. B. Toshmatov, D. Malafarina, N. Dadhich, Phys. Rev. D **100**, 044001 (2019)
56. C. Conde, C. Galvis, E. Larranaga, Phys. Rev. D **99**, 104059 (2019)
57. E. Larraaga, Int. J. Mod. Phys. D **29**, 2050121 (2020)
58. U. Nucamendi, R. Becerril, P. Sheoran, Eur. Phys. J. C **80**, 35 (2020)
59. C.A. Benavides-Gallego, W.B. Han, D. Malafarina et al., Phys. Rev. D **104**, 084024 (2021)
60. K. Yang, B.M. Gu, Y.P. Zhang, Eur. Phys. J. C **82**, 293 (2022)
61. S. Shaymatov, P. Sheoran, S. Siwach, Phys. Rev. D **105**, 104059 (2022)
62. J.M. Ladino, E. Larraaga, Int. J. Mod. Phys. D **31**, 2250091 (2022)
63. J. Li, C. Jiang, Mod. Phys. Lett. A **37**, 2250187 (2022)
64. F. Abdulxamidov, J. Rayimbaev, A. Abdujabbarov et al., Phys. Rev. D **108**, 044030 (2023)
65. K. Chen, S.W. Wei, Phys. Rev. D **110**, 024041 (2024)
66. T. Oteev, F. Abdulkhamidov, J. Rayimbaev et al., Phys. Dark Univ. **46**, 101588 (2024)
67. D. Umarov, F. Atamurotov, S.G. Ghosh et al., Eur. Phys. J. C **85**, 1 (2025)
68. T. Oteev, Z. Stuchlk, J. Rayimbaev et al., Eur. Phys. J. C **85**, 953 (2025)
69. S. Jumaniyozov, S.U. Khan, J. Rayimbaev et al., Phys. Rev. D **112**, 044068 (2025)
70. G. Rakhimova, F. Atamurotov, N. Juraeva et al., Phys. Dark Univ. **47**, 101721 (2025)
71. Y.B. Du, Y.L. Liu, X.D. Zhang, J. Cosmol. Astropart. Phys. **2025**, 045 (2025)
72. Q. Tan, W.K. Deng, S. Long et al., J. Cosmol. Astropart. Phys. **2025**, 044 (2025)
73. S. Jumaniyozov, J. Rayimbaev, Y. Turaev, Eur. Phys. J. C **85**, 1247 (2025)
74. M. Mathisson, Acta Phys. Pol. **6**, 163 (1937)
75. A. Papapetrou, Proc. R. Soc. A **209**, 248 (1951)
76. W.G. Dixon, Proc. R. Soc. A **314**, 499 (1970)